Kondo breakdown in the topological Kondo insulator SmB$_6$ studied by point-contact Andreev reflection spectroscopy

Masanobu Shiga [1,*] Tsubasa Teramoto,[1] Takurou Harada,[1] Takuya Takahashi,[1] Fumitoshi Iga [2] and Tatsuya Kawae[1,†]

[1]*Department of Applied Quantum Physics, Faculty of Engineering, Kyushu University, Motooka, Nishi-Ku, Fukuoka 819-0395, Japan*
[2]*Institute of Quantum Beam Science, Graduate School of Science and Engineering, Ibaraki University, Mito 310-8512, Japan*

We studied the topological features in Kondo insulator SmB$_6$ by point-contact Andreev reflection spectroscopy with a Nb probe tip. Below the superconducting transition of Nb, the spectra exhibited a narrow dip at around zero bias superposed on a broad asymmetric background caused by the Kondo resonance. The contact-size dependence of the spectra revealed that the width of the resonance is suppressed near the surface. The spin polarization in the surface state was ∼0.56, which is smaller than that in Bi-based topological insulators. These indicate that the Kondo breakdown plays a crucial role for the topological features, not only in the bulk state near the surface but also in the surface state on SmB$_6$.

I. INTRODUCTION

Three-dimensional (3D) topological insulators (TIs) are a newly developed class of insulators whose bulk is an insulator, whereas the surface is a two-dimensional metal protected by time-reversal symmetry, with a helically spin-polarized Dirac cone in the dispersion [1]. However, most 3D TIs do not exhibit bulk insulating properties [2], preventing their application as spintronic materials and the emergence of novel exotic phenomena such as Majorana fermions. Recently, theoretical studies have indicated that several Kondo insulators (KIs) can be understood as 3D TIs, referred to as topological Kondo insulators (TKIs) [3–5]. Importantly, a genuine bulk insulating state covered by a metallic surface state with a heavy Dirac quasiparticle is expected to appear at low temperatures in TKIs because the Fermi level lies in the hybridization gap generated by the strong hybridization between f and the conduction band (c-f hybridization) [3–7]. This indicates that TKIs are an optimal material for exploring the intrinsic features arising from the topologically protected surface state, although low temperatures are required to unfold their properties, which is a disadvantage for applications.

SmB$_6$ is known to exhibit the following novel features [3–7]. The electrical resistivity rapidly increases with decreasing temperature below the Kondo temperature owing to the formation of a hybridization gap near the Fermi level, which is typical of a KI [8–11]. However, it saturates below 4 K [8,9,12,13], which has recently been interpreted as the emergence of the expected metallic surface state in TKIs [3–7]. Indeed, several transport measurements of SmB$_6$ suggest the existence of a metallic surface state [14–18]. Moreover, the metallic surface state along with the hybridization gap

have been explored by various spectroscopic experiments, such as point-contact spectroscopy (PCS) [19–21], scanning tunneling spectroscopy (STS) [22–25], planar tunneling spectroscopy (PTS) [26–28], and angle-resolved photoemission spectroscopy (ARPES) [29–33] by probing the electronic density of states (DOS) near the Fermi level directly. These experiments indicate the formation of the topological Kondo state in SmB$_6$ as predicted by the theoretical studies [3–7]. However, the quantum oscillation [18] and ARPES measurements [30–33] show that the surface quasiparticles are light, which is inconsistent with the theories [3–7]. Recently, Alexandrov *et al.* proposed that this problem is resolved by considering the suppression of the Kondo effect at the surface, suggesting that the topological features in TKIs are varied in the vicinity of the surface due to the Kondo breakdown [34]. Indeed, the suppression of the Kondo effect was observed in the STS spectra of SmB$_6$ [23]. However, it is unclear whether the suppression occurs at the surface or in the bulk region, because the STS measurements probe the whole electronic state near the surface. This means that depth-dependent electronic DOS measurements are crucial for understanding the topological nature near the surface in TKIs.

To perform the depth-dependent investigation of the electronic DOS in SmB$_6$, we used point-contact Andreev reflection (PCAR) spectroscopy with a contact-size variation function at low temperatures. In the PCAR, differential conductance (dI/dV) spectra are recorded at the interface between a superconducting (SC) probe tip and a sample. If the applied bias voltage is smaller than the superconducting energy gap, the conductance dI/dV at the interface is governed by Andreev reflections [35]. Consequently, the spin polarization of the sample can be measured using PCAR. Spin polarization of the surface state has been estimated using PCAR measurements only on Bi-based TIs [36]. If the bias voltage exceeds the SC energy gap, the dI/dV spectra are proportional to the DOS of the sample, similar to the case of a

———————————
*shiga.masanobu.881@m.kyushu-u.ac.jp
†t.kawae.122@m.kyushu-u.ac.jp

normal-metal probe tip [37]. This implies that at the SC probe tip and the SmB$_6$ interface, the PCAR spectra above the SC energy gap reflect the hybridization gap formed near the Fermi energy owing to *c-f* hybridization. This enables studies of the spin-polarized surface state and the hybridization gap in the bulk state via PCAR measurements. Moreover, in the PCAR measurements, the depth dependence of the electronic DOS for the bulk and surface states were examined by changing the contact size between the SC probe tip and the SmB$_6$ interface.

In this paper, we report the PCAR spectroscopy investigation of SmB$_6$ using a Nb probe tip. Below the superconducting transition temperature of Nb, the spectra exhibited a narrow dip near zero bias, which overlapped with a broad asymmetric background. The background spectra are reproducible by a Fano curve, indicating the emergence of the Kondo resonance owing to *c-f* hybridization. The contact-size dependence of the spectra revealed that the magnitude of the Kondo resonance was suppressed in the vicinity of the surface. The spin polarization estimated from the narrow-dip structure below the SC energy gap was 0.56 ± 0.01, which is smaller than that of Bi-based TIs [36]. These features are explained by the Kondo breakdown arising from the suppression of *c-f* hybridization in the vicinity of the surface. Additionally, the decoupling between the 4*f* moments and the conduction electrons near the surface weakens the topological protected surface properties in TKIs.

II. EXPERIMENTAL DETAILS

A single-crystalline SmB$_6$ sample was grown using the floating-zone method in an image furnace with four xenon lamps [38]. The stoichiometric composition of SmB$_6$ was confirmed from the electrical resistivity and magnetic susceptibility measurements [39]. To study the Kondo breakdown, the surface state with a low Kondo temperature was investigated in the SmB$_6$ (100) plane [23]. Samples were cut along the (100) plane in air. After mechanical polishing, the sample was mounted on a ^{4}He cryostat. The experimental setup for the present PCAR spectroscopy measurements is the same as that of our previous PCS investigation, which was utilized to investigate the electronic DOS near the Fermi level of heavy fermion compounds with high energy resolution [40–43]. An Nb wire with a diameter of 0.2 mm (99.99%) was used as the probe tip. At $T \sim 4.3$ K, the probe tip was touched to the sample surface with a resistance below a dozen ohms to remove the effects of surface contamination, such as an oxidation layer, using an attocube positioner (ANPz51, attocube systems AG). Subsequently, the contact resistance between the probe tip and sample was controlled using a stacked-type piezoelectric device under a bias voltage larger than the SC energy gap. After preparing the contact, we focused on maintaining the contact during the measurements by controlling the stacked-type piezo device using a feedback loop. This procedure ensured that the PCAR spectra could be tracked without breaking the contact despite the wide variation in size during the measurements. The differential conductance dI/dV spectra were measured using lock-in amplifiers with a modulation frequency of $\omega = 1$ kHz and amplitude of approximately 0.05 mV.
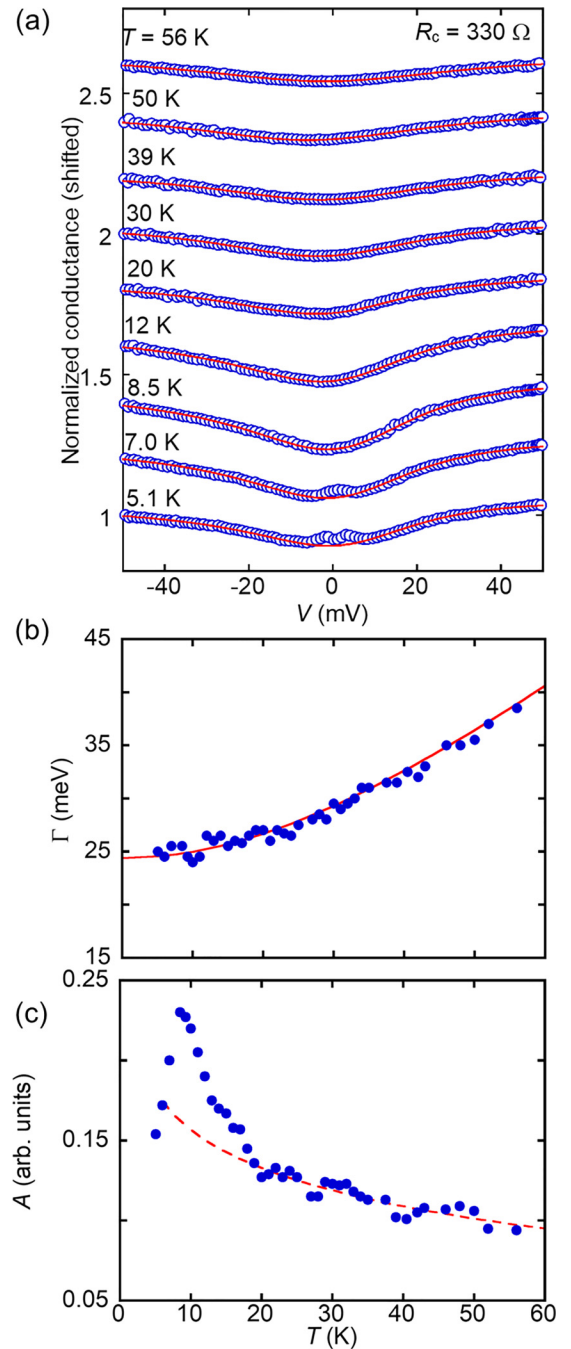

FIG. 1. (a) Temperature dependence of the PCAR spectra between SmB$_6$ and the Nb interface. The red solid line shows the fitting by the Fano model. (b), (c) Temperature dependence of the Γ and amplitude A obtained by fitting the PCAR spectra by the Fano model given by Eq. (1). The solid line is calculated using Eq. (3). The dashed line represents the logarithmic behavior.

III. RESULTS AND DISCUSSIONS

Figure 1(a) displays the temperature dependence of the PCAR spectra between $T = 5.1$ and 56 K. All the spectra in Fig. 1(a) are normalized by the amplitude at -50 mV. Below $T = 7.0$ K, an anomaly appears at around the zero bias, which overlaps with a broad asymmetric background. The asymmetric background is observed up to $T = 56$ K.

Similar asymmetric spectra have been observed in the PCS and STS spectra of SmB_6 using a normal-metal probe tip, where the spectra are reproduced using the Fano model [20–22,25]. Hence, we fitted the observed asymmetric spectra using the Fano model, which is expressed as follows:

$$G_F(V) = A\frac{(q+\varepsilon)^2}{1+\varepsilon^2}, \tag{1}$$

where the parameter ε is defined as

$$\varepsilon = \frac{eV - E_0}{\Gamma}. \tag{2}$$

Here, A, Γ, E_0, and q represent the amplitude, width of the asymmetric spectrum, center of the resonance, and Fano factor, respectively. q is defined as the ratio of probabilities between two tunneling paths, namely, for electrons tunneling from the probe tip to a discrete level and those tunneling from a continuous conduction band. The fittings by the Fano model are represented by the solid red lines in Fig. 1(a). In all the spectra, the asymmetric background is well reproduced by the Fano model despite the large temperature variation, indicating that the asymmetric background originates from the Fano resonance.

To clarify the origin of the Fano resonance, we estimated the temperature dependence of Γ and amplitude A from the fitting by the Fano model, as shown in Figs. 1(b) and 1(c). The results indicate that Γ increases with the temperature, which is typical of the Kondo resonance. In the Kondo resonance, the temperature dependence of Γ can be expressed by the following equation:

$$\Gamma = 2\sqrt{(\pi k_B T)^2 + 2(k_B T_K)^2}, \tag{3}$$

where T_K is the Kondo temperature [20,44]. The fitting performed using Eq. (3) is represented by the solid red line in Fig. 1(b). The experimental results were well reproduced using Eq. (3). Here, T_K was determined to be approximately 100 K, which is consistent with the value estimated from transport measurements [14]. Additionally, the amplitude of the Fano curve increases logarithmically with decreasing temperature [45] between 56 and 20 K, as shown by the red dashed line in Fig. 1(c). The observed features demonstrate that the asymmetric background originates from the Kondo resonance formed in the SmB_6 bulk state owing to c-f hybridization.

In a previous PCS study with an Ag-SmB_6 rigid-type junction, an asymmetric double peak structure was observed, which was explained by the formation of a hybridization gap in the electronic DOS predicted by the theory [20,46]. In contrast, in many PCS and STS spectra of SmB_6, the asymmetric background structure is reproduced by Fano resonance [21,22,25]. This discrepancy could arise from the difference in the junction size. STS measurements can be used to obtain the local electronic DOS with atomic size resolution on the sample surface. However, in PCS measurements, the spectra reflect the averaged DOS within the point contact. The contact size of approximately 100 μm used in the previous study [20] is considerably larger than that used in the present study as will be discussed in Fig. 3, which suggests the junction size affects the spectral shape of PCS spectra. Importantly, the width

of the asymmetric spectrum was in good agreement with the peak separation of the asymmetric double peak. Thus, it is reasonable to consider that the hybridization gap formed in the electronic DOS is responsible for the asymmetric spectra in SmB_6.

Significantly, the amplitude rapidly increased below 20 K, implying a change in the electronic DOS near the Fermi level. According to spin-resolved APRES experiments, a spin-polarized metallic surface state is observed at approximately 20 K [33]. This strongly suggests that the increase in amplitude occurs owing to the emergence of a metallic surface state. Below $T = 7$ K, the amplitude decreased steeply, which is related to the SC transition of the Nb probe tip.

Next, we discuss the origin of the dip-shaped zero-bias anomaly in the PCAR spectra below 7.0 K. This anomaly appeared below the SC transition of Nb, indicating that it can be explained by the Andreev reflection between the metallic surface state on SmB_6 and the SC Nb tip interface [35]. Importantly, the dip-shaped spectrum exhibits the suppression of the Andreev reflection, indicating the existence of a spin-polarized state on SmB_6 as described below. Because each electron of a Cooper pair in the probe tip has a finite vertical projection of its spin, the Cooper-pair spins are aligned along the perpendicular wave vector k_Z in the ballistic regime of PCAR spectroscopy. In TIs, the electron spins in the metallic surface state are locked onto the in-plane wave vectors k_x and k_y. Hence, the injection of Cooper pairs with spins along the z direction into the TIs is not allowed because of momentum conservation within the elastic limit. Consequently, the Andreev reflection was suppressed owing to the spin polarization of the surface state on the TIs. The high spin polarization of the Bi-based TIs $(Bi_{1-x}Sb_x)_2Te_3$ was confirmed by PCAR spectroscopy [36].

The dip-shaped zero-bias anomaly was evident below $T = 7.0$ K, which was considerably lower than the SC transition temperature of bulk Nb ($T_c = 9.2$ K). This represented an increase in the effective temperature near the SmB_6/Nb interface by the Joule heating during the measurements, which prevented an accurate evaluation of the spin polarization of the surface state by PCAR. Therefore, we lowered the amplitude of the sweep bias voltage in the subsequent measurements.

Figure 2(a) shows the contact-resistance dependence, namely, the contact-size dependence, of the PCAR spectra for a bias voltage of $|V|20\,mV$ at $T = 4.5$ K. The spectra are normalized to the amplitude at $V = -20\,mV$. In all the spectra, the dip-shaped zero-bias anomaly overlaps with an asymmetric background, indicating that the coexistence of the two features is intrinsic for PCAR spectra on SmB_6. As described previously, the asymmetric background can be fitted using the Fano model, which is depicted by the solid red lines in Fig. 2(a). The dip-shaped zero-bias anomaly originated from the Andreev reflection between the SC Nb tip and the spin-polarized surface state of SmB_6. Hence, the polarization was evaluated based on the modified Blonder-Thinkham-Klapwijk (m-BTK) model [47], which was used to evaluate the spin polarization in a ferromagnet from the suppression of the Andreev reflection between a superconductor and ferromagnetic material interface [48–51]. Subsequently, it was confirmed that the m-BTK model could be applied to evaluate the spin polarization of TI [36].
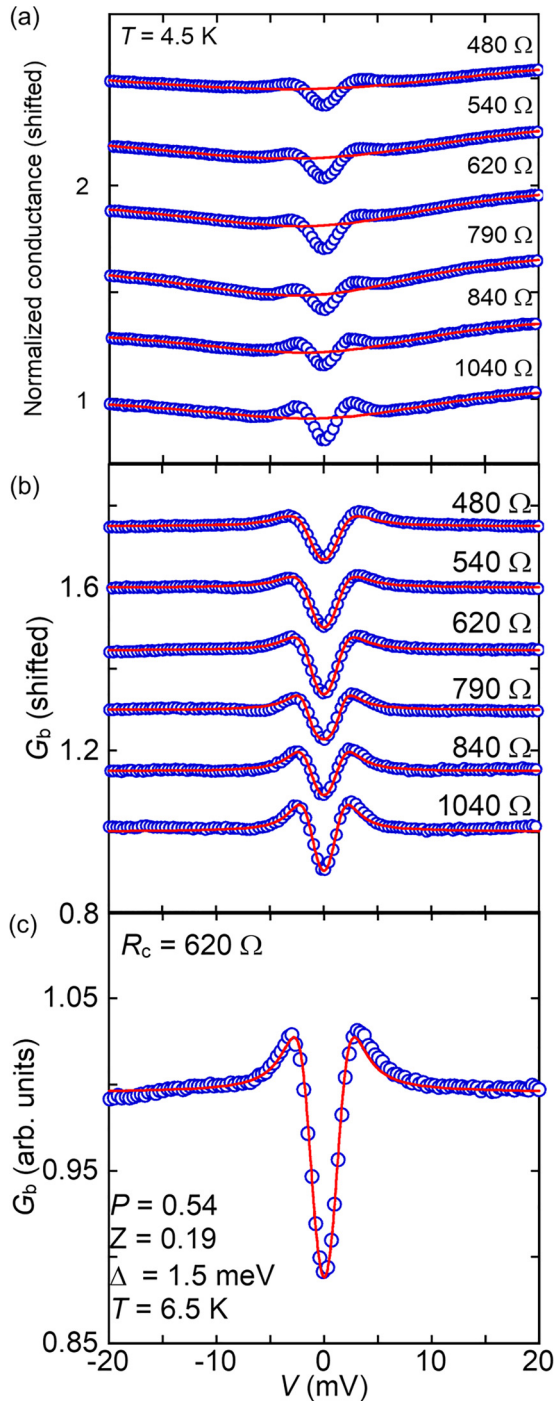
FIG. 2. (a) Contact-resistance dependence of the PCAR spectra between SmB_6 and the Nb interface at $T = 4.5$ K. The decrease of the resistance corresponds to the increase in the contact size. The solid lines represent the fitting by the Fano model. (b) Fitting of the G_b, which is a spectrum after subtracting the asymmetric background using the Fano model, by the m-BTK model. (c) Fitting of the G_b at $R_c = 620\ \Omega$ by the m-BTK model, where the fitting parameters are shown in the figure.

FIG. 3. (a) Contact-resistance dependence of the width of the asymmetric background Γ estimated using the Fano model. The decrease of the resistance corresponds to the increase in the contact size. (b) Contact-size dependence of the spin polarization P and interface scattering parameter Z evaluated by the m-BTK model, where P and Z are depicted by the blue circles and red triangles, respectively.

spectrum by fitting the Fano curve. Subsequently, the spectra were fitted by the m-BTK model, which included four fitting parameters: spin polarization P, interface scattering parameter Z, temperature T, and the superconducting energy gap Δ. As shown by the red solid lines in Fig. 2(b), all the spectra are well reproduced by the m-BTK model using $P \sim 0.5$, demonstrating that a spin-polarized metallic state exists on the surface of SmB_6. In contrast, the fitting parameter T is considered as $T \sim 6.5$ K as shown in Fig. 2(c), which is higher than the experimental temperature $T = 4.5$ K. This indicates the involvement of local heating effects in the spectra for a sweep amplitude of $|V| = 20$ mV. However, the existence of the high-spin polarized state despite the temperature increase owing to heating is crucial [36].

Figure 3 shows the contact resistance R_c dependence of the width of the Kondo resonance Γ, spin polarization P, and interface scattering parameter Z, which are estimated by fitting the Fano and m-BTK models, as described in Fig. 2. As shown in Fig. 3(a), Γ decreases with increasing R_c, namely, with decreasing contact size. In the Kondo lattice systems, such as $EuNi_2P_2$, YbPd, and CeB_6, the electronic properties of the $4f$ state are not affected by the contact size in the PCS

Before the zero-bias anomaly was fitted using the m-BTK model, the asymmetric background was subtracted from the observed spectra. Figure 2(b) shows the spectrum G_b after subtracting the asymmetric background from the observed
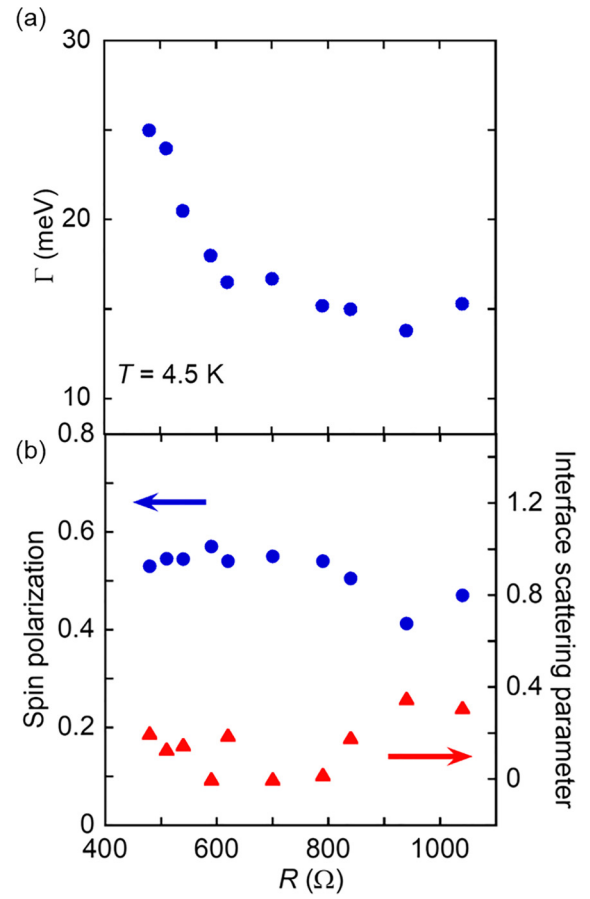
measurements [40–43], strongly suggesting that the contact-size dependence of the spectra reflects intrinsic properties of Γ in SmB_6. Indeed, at a large R_c, the value of Γ is estimated to be 15 meV, which is in good agreement with that of the nonreconstructed clean SmB_6 (100) surface obtained by STS measurements [22]. These indicate that the observed spectra are not affected by defects and/or roughness on the surface. The value of $\Gamma \sim 25$ meV at a small R_c in Fig. 3(a) is consistent with that of the sweep amplitude $|V| = 50$ mV in Fig. 1, meaning that Γ can be estimated from the PCAR spectra despite decreasing the amplitude of the sweep bias voltage to $|V| = 20$ mV. Here, we estimated the contact size by assuming the Sharvin relation $R_s = 16l\rho_s/3d^2\pi$ [37], where the l, ρ_s, and d represent electron mean free path, electrical resistivity of surface state, and contact diameter, respectively. Considering $l \sim 20$ nm and $\rho \sim 9.4 \times 10^{-5}$ Ω cm [18,52], the contact diameters (d) at the maximum and minimum resistance of $R_c = 1040$ and 480 Ω in Fig. 2(a) were estimated to be approximately 5 nm and approximately 8 nm, respectively. A previous study by Lee *et al.* estimated the thickness of the metallic surface layer on SmB_6 to be approximately 6 nm [52]. Because the depth of the probe tip in the PCS measurements is approximately the same size as the contact diameter, the spectra for $R_c \gtrsim 1000$ Ω primarily reflects the electronic DOS of the surface layer.

The above facts indicate that the PCS spectra of SmB_6 originated from the surface and bulk states for $R_c < 1000$ Ω, where the depth of the probe tip exceeded the surface thickness. Therefore, the spectral shape was expected to vary with the contact size if the electronic DOS for the surface and bulk states were different. Therefore, the decrease of Γ at small contact sizes, i.e., large contact resistances, in Fig. 3(a) indicates the suppression of the c-f hybridization in the vicinity of SmB_6 surface. In other words, the Kondo breakdown occurs in the vicinity of the SmB_6 surface. From the theoretical and experimental studies, several possibilities, such as the reduced coordination of Sm ions, oxidation, chemical damage, and Sm vacancy at the SmB_6 surface, are considered as the origin of the Kondo breakdown [34,53–56]. To reveal the origin of Kondo breakdown in the vicinity of the surface, further investigations are needed.

Unlike Γ, the spin polarizations P and Z did not vary significantly when the contact resistance changed, as shown in Fig. 3(b). The slight variation in P, which decreases with increasing resistance, could result from the altered potential barrier at the SmB_6/Nb interface. Similar features have been observed in ferromagnetic materials [49,51]. Based on the contact-resistance dependence of Γ, P, and Z, it is reasonable to assume that the surface state covers the bulk Kondo state.

As described above, the local heating effect continued to occur in the measurements when the amplitude of the sweep bias voltage was $|V| = 20$ mV. Therefore, we further decreased the sweep amplitude to $|V| = 10$ mV to eliminate heating effects during the measurements. Figure 4(a) illustrates the PCAR spectra at $T = 4.5$ K, where the asymmetric background overlapping with the dip-shaped zero-bias anomaly is clearly observed, although the sweep amplitude decreases from $|V| = 20$ mV to 10 mV. We fit the background
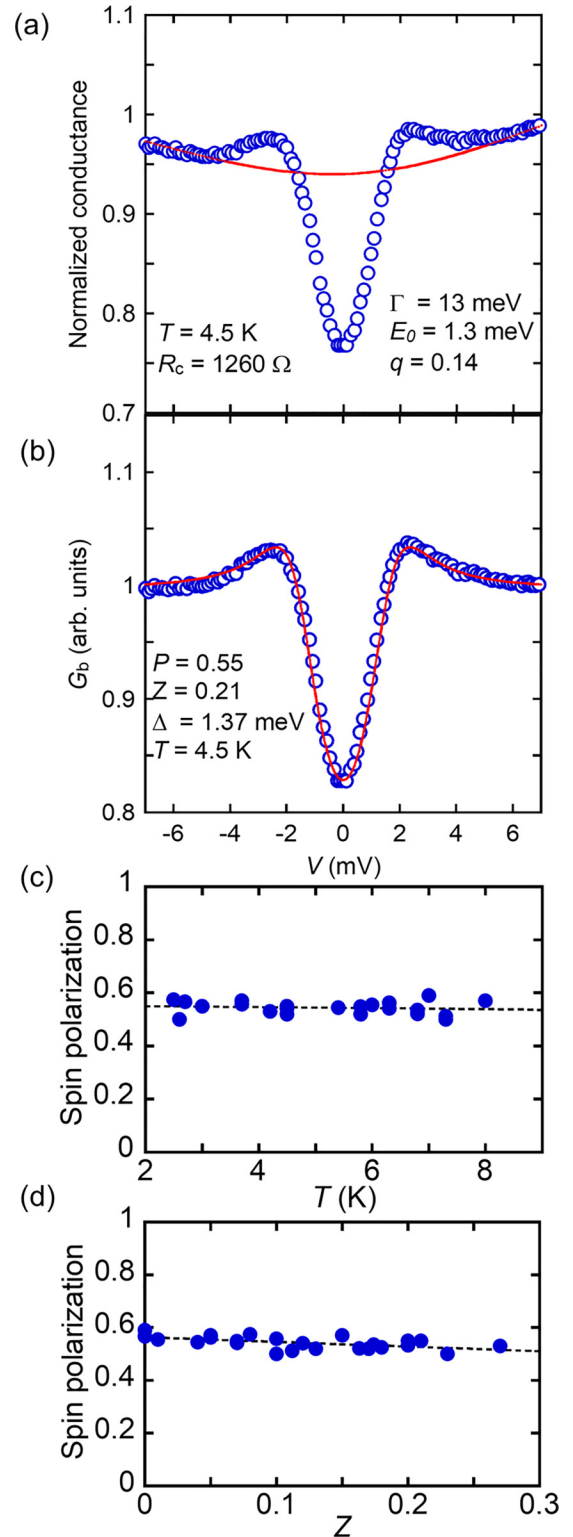

FIG. 4. (a), (b) PCAR spectrum at $T = 4.5$ K fitted by the Fano and m-BTK models, respectively. (c) Temperature dependence of the spin polarization evaluated by the m-BTK model. The dashed line represents the linear extrapolation. (d) The spin polarization as a function of the interface scattering parameter Z. The spin polarization at $Z = 0$ is estimated to be 0.56 ± 0.01 from the linear extrapolation as shown by the dashed line.

using the Fano model estimated from the PCAR measurements of $|V| \geqslant 20$ mV, which are depicted by the red solid line in Fig. 4(a). Figure 4(b) shows the spectrum G_b after subtracting the background, which is well reproduced by fitting based on the m-BTK model with a spin polarization value of $P = 0.55$, as depicted by the red solid line. Moreover, the fitting temperature was consistent with the experimental temperature for the sweep amplitude of $|V| = 10$ mV, indicating the suppression of heating during the measurements. The value of P was consistent with that for $|V| = 20$ mV [Fig. 2(c)], indicating that the polarization was unaffected by heating during the measurements. The temperature dependence of the spin polarization is shown in Fig. 4(c), in which the polarization is evaluated above a contact resistance of 1000 Ω to reduce the effect of the bulk state. These results demonstrate that below $T \sim 8$ K, the spin polarization of the metallic surface state on SmB_6 is independent of temperature. In the PCAR investigation between a polycrystalline SmB_6 film and Nb interface, the spectra were reproduced by the BTK model [57], suggesting that a spin polarization is suppressed on the SmB_6 surface. At low temperatures, the bulk properties in SmB_6 are varied significantly by the existence of disorders in the crystal [58]. Similarly, the surface properties, such as spin polarization, could be affected by disorders of the sample [28].

Finally, we discuss the intensity of the spin polarization for the surface state in SmB_6. Because SmB_6 is a TKI, it is natural for a high-spin polarization state to be confirmed by the PCAR spectra, as in the case of Bi-based TIs $(Bi_{1-x}Sb_x)_2Te_3$ [36], where the spin polarizations in Bi_2Te_3 and in Sb_2Te_3 are reported to be $P \sim 0.7$ at $Z \sim 0.3$ and $P \sim 0.57$ at $Z \sim 0.6$, respectively. In SmB_6, the spin polarization at $Z = 0$ is given as $P = 0.56 \pm 0.01$ in Fig. 4(d). Generally, the spin polarization decreases with increasing Z [49–51], meaning that the polarization at $Z = 0$ in $(Bi_{1-x}Sb_x)_2Te_3$ is much larger that of the above values. These imply that the spin polarization in SmB_6 is smaller than that in $(Bi_{1-x}Sb_x)_2Te_3$ owing to the suppression of c-f hybridization at the SmB_6 surface. As shown in Fig. 3, the Kondo resonance in the vicinity of the surface narrows owing to the Kondo breakdown arising from the suppression of the hybridization. This indicates decoupling between the localized $4f$ moments and conduction electrons in the vicinity of the surface. The decoupling also reduces the spin polarization because the topological future of the surface state originates from the hybridization in SmB_6. Namely, the Kondo breakdown in the vicinity of the surface leads to incompletion of the topologically protected surface state in SmB_6. Meanwhile, according to the previous theoretical and experimental studies, the spin excitons in SmB_6 suppress the topological nature of the surface state [26–28,59]. Therefore, to clarify the suppression of spin polarization at the surface state in TKIs, further theoretical and experimental investigation is required.

IV. CONCLUSION

In conclusion, we conducted a PCAR spectroscopic investigation of SmB_6 using an Nb tip. Below the superconducting transition temperature of Nb, the PCAR spectra were decomposed into two components: a narrow-dip structure at approximately zero bias arising from the Andreev reflection between the spin-polarized surface state on the SmB_6 and SC Nb interfaces, and a broad asymmetric background owing to the formation of the Kondo resonance. The contact-size dependence of the spectra revealed that the width of the Kondo resonance was narrowed as the contact size decreased. This is caused by the Kondo breakdown arising from the suppression of c-f hybridization owing to the reduced coordination of the Sm^{3+} ions in the vicinity of the surface. The spin polarization is smaller than that of the Bi-based TI, which is understood as the decoupling between the $4f$ moments and conduction electrons due to the Kondo breakdown. The results strongly suggest that in TKI the Kondo breakdown plays a crucial role for the topological features, not only in the bulk state in the vicinity of the surface but also in the surface state.

[1] M. Z. Hasan and C. L. Kane, *Colloquium*: Topological insulators, Rev. Mod. Phys. **82**, 3045 (2010).

[2] Y. Ando, Topological insulator materials, J. Phys. Soc. Jpn. **82**, 102001 (2013).

[3] M. Dzero, K. Sum, V. Galitski, and P. Coleman, Topological Kondo insulators, Phys. Rev. Lett. **104**, 106408 (2010).

[4] M. Dzero, K. Sun, P. Coleman, and V. Galitski, Theory of topological Kondo insulators, Phys. Rev. B **85**, 045130 (2012).

[5] V. Alexandrov, M. Dzero, and P. Coleman, Cubic topological Kondo insulators, Phys. Rev. Lett. **111**, 226403 (2013).

[6] T. Takimoto, A promising candidate for a topological insulator, J. Phys. Soc. Jpn. **80**, 123710 (2011).

[7] F. Lu, J. Z. Zhao, H. Weng, Z. Fang, and X. Dai, Correlated topological insulators with mixed valence, Phys. Rev. Lett. **110**, 096401 (2013).

[8] J. C. Nickerson, R. M. White, K. N. Lee, R. Bachmann, T. H. Geballe, and G. W. Hull Jr., Physical properties of SmB_6, Phys. Rev. B **3**, 2030 (1971).

[9] J. W. Allen, B. Batlogg, and P. Wachter, Large low-temperature Hall effect and resistivity in mixed-valence SmB_6, Phys. Rev. B **20**, 4807 (1979).

[10] G. Travaglini and P. Wachter, Intermediate-valent SmB_6 and the hybridization model: An optical study, Phys. Rev. B **29**, 893 (1984).

[11] S. I. Kimura, T. Nanba, S. Kunii, and T. Kasuya, Low-energy optical excitation in rare-earth hexaborides, Phys. Rev. B **50**, 1406 (1994).

[12] S. Wolgast, Ç. Kurdak, K. Sun, J. W. Allen, D.-J. Kim, and Z. Fisk, Low-temperature surface conduction in the Kondo insulator SmB_6, Phys. Rev. B **88**, 180405(R) (2013).

[13] P. Syers, D. Kim, M. S. Fuhrer, and J. Paglione, Tuning bulk and surface conduction in the proposed topological Kondo insulator SmB_6, Phys. Rev. Lett. **114**, 096601 (2015).

[14] W. A. Phelan, S. M. Koohpayeh, P. Cottingham, J. W. Freeland, J. C. Leiner, C. L. Broholm, and T. M. McQueen, Correlation between bulk thermodynamic measurements and the low-temperature-resistance plateau in SmB_6, Phys. Rev. X **4**, 031012 (2014).

[15] F. Chen, C. Shang, Z. Jin, D. Zhao, Y. P. Wu, Z. J. Xiang, Z. C. Xia, A. F. Wang, X. G. Luo, T. Wu, and X. H. Chen, Magnetoresistance evidence of a surface state and a field-dependent insulating state in the Kondo insulator SmB_6, Phys. Rev. B **91**, 205133 (2015).

[16] S. Thomas, D. J. Kim, S. B. Chung, T. Grant, Z. Fisk, and J. Xia, Weak antilocalization and linear magnetoresistance in the surface state of SmB_6, Phys. Rev. B **94**, 205114 (2016).

[17] Q. Song, J. Mi, D. Zhao, T. Su, W. Yuan, W. Xing, Y. Chen, T. Wang, T. Wu, X. H. Chen, X. C. Xie, C. Zhang, J. Shi, and W. Han, Spin injection and inverse Edelstein effect in the surface states of topological Kondo insulator SmB_6, Nat. Commun. **7**, 13485 (2016).

[18] G. Li, Z. Xiang, F. Yu, T. Asaba, B. Lawson, P. Cai, C. Tinsman, A. Berkley, S. Wolgast, Y. S. Eo, D.-J. Kim, C. Kurdak, J. W. Allen, K. Sun, X. H. Chen, Y. Y.Wang, Z. Fisk, and Lu Li, Two-dimensional Fermi surface in Kondo insulator SmB_6, Science **346**, 1208 (2014).

[19] I. Frankowski and P. Wachter, Point-contact spectroscopy on SmB_6, TmSe, LaB_6, and LaSe, Solid State Commun. **41**, 577 (1982).

[20] X. Zhang, N. P. Butch, P. Syers, S. Ziemak, R. L. Greene, and J. Paglione, Hybridization, inter-ion correlation, and surface state in the Kondo insulator SmB_6, Phys. Rev. X **3**, 011011 (2013).

[21] T. Harada, M. Shiga, K. Okimura, Y. Inagaki, F. Iga, and T. Kawae, Point-contact spectroscopy study of Kondo insulator SmB_6, JPS Conf. Proc. **30**, 011022 (2020).

[22] S. Rößler, T.-H. Jang, D.-J. Kim, L. H. Tjeng, Z. Fisk, F. Steglich, and S. Wirth, Hybridization gap and Fano resonance in SmB_6, Proc. Natl. Acad. Sci. USA **111**, 4798 (2014).

[23] L. Jiao, S. Rößler, D. J. Kim, L. H. Tjeng, Z. Fisk, F. Steglich, and S. Wirth, Additional energy scale in SmB_6 at low-temperature, Nat. Commun. **7**, 13762 (2016).

[24] L. Jiao, S. Rößler, D. Kasinathan, P. F. S. Rosa, C. Guo, H. Yuan, C.-X. Liu Z. Fisk, F. Steglich, and S. Wirth, Magnetic and defect probes of the SmB_6 surface state, Sci. Adv. **4**, eaau4886 (2018).

[25] H. Pirie, Y. Liu, A. Soumyanarayanan, P. Chen, Y. He, M. M. Yee, P. F. S. Rosa, J. D. Thompson, D.-J. Kim, Z. Fisk, J. Paglione X.Wang, D. K. Morr, M. H. Hamidian, and J. E. Hoffman, Imaging emergent heavy Dirac fermions of a topological Kondo insulator, Nat. Phys. **16**, 52 (2020).

[26] W. K. Park, L. Sun, A. Noddings, D.-J. Kim, Z. Fisk, and L. H. Greene, Topological surface states interacting with bulk excitations in the Kondo insulator SmB_6 revealed via planar tunneling spectroscopy, Proc. Natl. Acad. Sci. USA **113**, 6599 (2016).

[27] L. Sun, D.-J. Kim, Z. Fisk, and W. K. Park, Planar tunneling spectroscopy of the topological Kondo insulator SmB_6, Phys. Rev. B **95**, 195129 (2017).

[28] W. K. Park, J. A. Sittler, L. H. Greene, W. T. Fuhrman, J. R. Chamorro, S. M. Koohpayeh, W. A. Phelan, and T. M.

McQueen, Topological nature of the Kondo insulator SmB_6 and its sensitiveness to Sm vacancy, Phys. Rev. B **103**, 155125 (2021).

[29] H. Miyazaki, T. Hajiri, T. Ito, S. Kunii, and S. Kimura, Momentum-dependent hybridization gap and dispersive in-gap state of the Kondo semiconductor SmB_6, Phys. Rev. B **86**, 075105 (2012).

[30] N. Xu, X. Si, P. K. Biswas, C. E. Matt, R. S. Dhaka, Y. Huang, N. C. Plumb, M. Radović, J. H. Dil, E. Pomjakushina, K. Conder, A. Amato, Z. Salman, D. McK. Paul, H. Ding, and M. Shi, Surface and bulk electronic structure of the strongly correlated system SmB_6 and implications for a topological Kondo insulator, Phys. Rev. B **88**, 121102(R) (2013).

[31] M. Neupane, N. Alidoust, S-Y. Xu, T. Kondo, Y. Ishida, D. J. Kim, C. Liu, I. Belopolski, Y. J. Jo, T.-R. Chang, H.-T. Jeng, T. Durakiewicz, L. Balicas, H. Lin, A. Bansil, S. Shin, Z. Fisk, and M. Z. Hasan, Surface electronic structure of the topological Kondo-insulator candidate correlated electron system SmB_6, Nat. Commun. **4**, 2991 (2013).

[32] J. Jiang, S. Li, T. Zhang, Z. Sun, F. Chen, Z. R. Ye, M. Xu, Q. Q. Ge, S. Y. Tan, X. H. Niu, M. Xia, B. P. Xie, Y. F. Li, X. H. Chen, H. H. Wen, and D. L. Feng, Observation of possible topological in-gap surface states in the Kondo insulator SmB_6 by photoemission, Nat. Commun. **4**, 3010 (2013).

[33] N. Xu, P. K. Biswas, J. H. Dil, R. S. Dhaka, G. Landolt, S. Muff, C. E. Matt, X. Shi, N. C. Plumb, M. Radović, E. Pomjakushina, K. Conder, A. Amato, S. V. Borisenko, R. Yu, H.-M. Weng, Z. Fang, X. Dai, J. Mesot, H. Ding, and M. Shi, Direct observation of the spin texture in SmB_6 as evidence of the topological Kondo insulator, Nat. Commun. **5**, 4566 (2014).

[34] V. Alexandrov, P. Coleman, and O. Erten, Kondo breakdown in topological insulator, Phys. Rev. Lett. **114**, 177202 (2015).

[35] G. E. Blonder, M. Tinkham, and T. M. Klapwijk, Transition from metallic to tunneling regime in superconducting microconstrictions: Excess current, charge imbalance, and supercurrent conversion, Phys. Rev. B **25**, 4515 (1982).

[36] K. Borisov, C.-Z. Chang, J. S. Moodera, and P. Stamenov, High Fermi-level spin polarization in the $(Bi_{1-x}Sb_x)_2Te_3$ family of topological insulators: A point contact Andreev reflection study, Phys. Rev. B **94**, 094415 (2016).

[37] Y. G. Naidyuk and I. K. Yanson, *Point-Contact Spectroscopy* (Springer, New York, 2005).

[38] F. Iga, N. Shimizu, and T. Takabatake, Single crystal growth and physical properties of Kondo insulator YbB_{12}, J. Magn. Magn. Mater. **177**, 337 (1998).

[39] D. Nakamura, A. Miyake, A. Ikeda, M. Tokunaga, F. Iga, and Y. H. Matsuda, Closing the hybridization charge gap in the Kondo semiconductor SmB_6 with an ultrahigh magnetic field, Phys. Rev. B **105**, L241105 (2022).

[40] M. Shiga, K. Okimura, H. Takata, A. Mitsuda, I. Maruyama, H. Wada, Y. Inagaki, and T. Kawae, Observation of Kondo resonance in valence-ordered YbPd, Phys. Rev. B **100**, 245117 (2019).

[41] M. Shiga, T. Harada, T. Takahashi, A. Mitsuda, H. Wada, Y. Inagaki, and T. Kawae, Point-contact spectroscopy study of YbPd/W interface, JPS Conf. Proc. **30**, 011139 (2020).

[42] M. Shiga, I. Maruyama, K. Okimura, T. Harada, T. Takahashi, A. Mitsuda, H. Wada, Y. Inagaki, and T. Kawae, Evolution

of lattice coherence in the intermediate-valence heavy-fermion compound $EuNi_2P_2$ studies by point contact spectroscopy, Phys. Rev. B **103**, L041113 (2021).

[43] M. Shiga, T. Takahashi, T. Teramoto, F. Iga, and T. Kawae, Observation of Kondo resonance and low-energy excitation in CeB_6 using point-contact spectroscopy, J. Phys. Soc. Jpn. **91**, 113705 (2022).

[44] K. Nagaoka, T. Jamneala, M. Grobis, and M. F. Crommie, Temperature dependence of a single Kondo impurity, Phys. Rev. Lett. **88**, 077205 (2002).

[45] S. M. Cronenwett, T. H. Oosterkamp, and L. P. Kouwenhoven, A tunable Kondo effect in quantum dots, Science **281**, 540 (1998).

[46] M. Maltseva, M. Dzero, and P. Coleman, Electron cotunneling into a Kondo Lattice, Phys. Rev. Lett. **103**, 206402 (2009).

[47] I. I. Mazin, A. A. Golubov, and B. Nadgorny, Probing spin polarization with Andreev reflection: A theoretical basis, J. Appl. Phys. **89**, 7576 (2001).

[48] R. J. Soulen Jr., J. M. Byers, M. S. Osofsky, B. Nadgorny, T. Ambrose, S. F. Cheng, P. R. Broussard, C. T. Tanaka, J. Nowak, J. S. Moodera, A. Barry, and J. M. D. Coey, Measuring the spin polarization of a metal with a superconducting point contact, Science **282**, 85 (1998).

[49] Y. Ji, G. J. Strijkers, F. Y. Yang, C. L. Chien, J. M. Byers, A. Anguelouch, G. Xiao, and A. Gupta, Determination of the spin polarization of half-metallic CrO_2 by point contact andreev reflection, Phys. Rev. Lett. **86**, 5585 (2001).

[50] B. Nadgorny, I. I. Mazin, M. Osofsky, R. J. Soulen Jr., P. Broussard, R. M. Stroud, D. J. Singh, V. G. Harris, A. Arsenov, and Ya. Mukovskii, Origin of high transport spin polarization in $La_{0.7}Sr_{0.3}MnO_3$: Direct evidence for minority spin state, Phys. Rev. B **63**, 184433 (2001).

[51] M. Shiga, N. Nishimura, Y. Inagaki, T. Kawae, H. Kambara, and K. Tenya, Spin polarization measurements in ferromagnetic $SrRuO_3$ using point-contact Andreev reflection technique, J. Phys.: Conf. Ser. **807**, 082001 (2017).

[52] S. Lee, X. Zhang, Y. Liang, S. W. Fackler, J. Yong, X. Wang, J. Paglione, R. L. Greene, and I. Takeuchi, Observation of the superconducting proximity effect in the surface state of SmB_6 thin films, Phys. Rev. X **6**, 031031 (2016).

[53] J. W. Allen, Foreward for special issue of philosophical magazine on: Topological correlated insulators and SmB_6, Philos. Mag. **96**, 3227 (2016).

[54] P. Lutz, M. Thees, T. R. F. Peixoto, B. Y. Kang, B. K. Cho, C.-H. Min, and F. Reinert, Valence characterization of surface and subsurface region in SmB_6, Philos. Mag. **96**, 3307 (2016).

[55] Y. Utsumi, D. Kasinathan, K.-T. Ko, S. Agrestini, M. W. Haverkort, S. Wirth, Y-H. Wu, K-D. Tsuei, D-J. Kim, Z. Fisk, A. Tanaka, P. Thalmeier, and L. H. Tjeng, Bulk and surface electronic properties of SmB_6: A hard x-ray photoelectron spectroscopy study, Phys. Rev. B **96**, 155130 (2017).

[56] C. E. Matt, H. Pirie, A. Soumyanarayanan, Y. He, M. M. Yee, P. Chen, Y. Liu, D. T. Larson, W. S. Paz, J. J. Palacios, M. H. Hamidian, and J. E. Hoffman, Consistency between ARPES and STM measurements on SmB_6, Phys. Rev. B **101**, 085142 (2020).

[57] J. Yong, Y. Jiang, D. Usanmaz, S. Curtarolo, X. Zhang, L. Li, X. Pan, J. Shin, I. Takeuchi, and R. L. Greene, Robust topological surface state in Kondo insulator SmB_6 thin films, Appl. Phys. Lett. **105**, 222403 (2014).

[58] Y. S. Eo, A. Rakoski, S. Sinha, D. Mihaliov, W. T. Fuhrman, S. R. Saha, P. F. S. Rosa, Z. Fisk, M. C. Hatnean, G. Balakrishnan, J. R. Chamorro, W. A. Phelan, S. M. Koohpayeh, T. M. McQueen, B. Kang, M.-S. Song, B. Cho, M. S. Futhrer, J. Paglione, and Ç. Kurdak, Bulk transport paths through defects in floating zone and Al flux grown SmB_6, Phys Rev. Mater. **5**, 055001 (2021).

[59] G. A. Kapilevich, P. S. Riseborough, A. X. Gray, M. Gulacsi, T. Durakiewicz, and J. L. Smith, Incomplete protection of the surface Weyl cones of the Kondo insulator SmB_6: Spin exciton scattering, Phys. Rev. B **92**, 085133 (2015).